GA–A24452

COMPLETE SURFACE MAPPING OF ICF SHELLS

by
R.B. STEPHENS, D. OLSON, H. HUANG,
and J.B. GIBSON

SEPTEMBER 2003

DISCLAIMER

GA–A24452

COMPLETE SURFACE MAPPING OF ICF SHELLS

by
R.B. STEPHENS, D. OLSON, H. HUANG,
and J.B. GIBSON

This is a preprint of a paper presented at the 15th Target Fabricartion Specialists Meeting, Gleneden Beach, Oregon, June 1–5, 2003 and to be published in *Fusion Science and Technology.*

Work supported by
the U.S. Department of Energy
under Contract No. DE-AC03-01SF22260

GENERAL ATOMICS PROJECT 30095
SEPTEMBER 2003

COMPLETE SURFACE MAPPING OF ICF SHELLS

R.B. Stephens, D. Olson, H. Huang, and J.B. Gibson
email: rich.stephens@gat.com

General Atomics, P.O. Box 85608, San Diego, California 92186-5608

Inertial confinement fusion shells have previously been evaluated on the basis of microscopic examination for local defects and limited surface profiling to represent their average fluctuation power. Since defects are local, and don't always have visible edges, this approach both misses some important fluctuations and doesn't properly represent the spatially dependent surface fluctuation power. We have taken the first step toward correcting this problem by demonstrating the capability to completely map the surface of a NIF shell with the resolution to account for all modes. This allows complete accounting of all the surface fluctuations. In the future this capability could be used for valuable shells to generate a complete $r(\theta,\phi)$ surface map for accurate 3-D modeling of a shot.

I. INTRODUCTION

The outside of inertial confinement fusion (ICF) shells is Rayleigh-Taylor unstable during compression. Deviations from spherical symmetry will grow rapidly, feed through to the inside surface and, potentially, quench the central hot spot.[1] An error budget has been established for the National Ignition Facility (NIF) that includes an average fluctuation power spectra for the shell surface (Fig. 1).[2] Recently a specification has been added for isolated defects.[3]

Surface analysis techniques have not been adequate to satisfy these specs. The standard procedure is to microscopically cull shells with visible defects and then to calculate the fluctuation power of the remainder from the average of the Fourier Transform of nine shell profiles, taken along three parallel traces (separated by ~ 10 μm) in three mutually orthogonal great circles [Fig. 2(a)]. The optical examination detects flaws with sharply defined edges, but many local defects are completely invisible by such technique (such as the bumps and hollows shown in Fig. 2(b). The standard profiles examine the surface in great detail, for modes up to ~1800 along lines ~20 μm

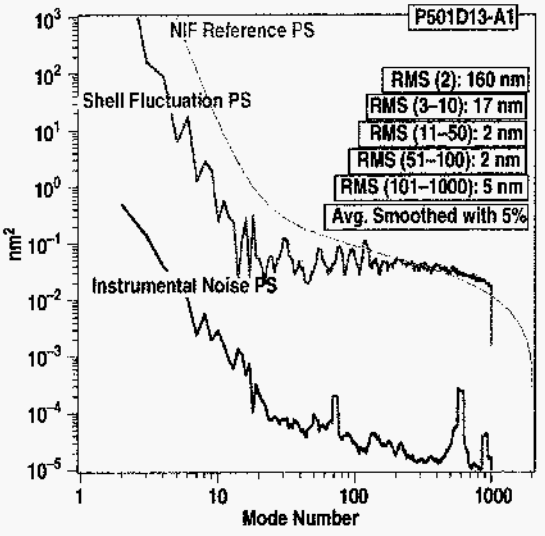

Fig. 1. Sphere surface fluctuation power versus mode number showing instrumental limit for power spectrum measurements, a shell power spectrum, and the NIF reference, which is the limit for acceptance. Both experimental spectra were smoothed using a 5% wide boxcar average.

wide, surrounding eight large areas that are completely unexamined. The probability of this pattern detecting a local defect depends on the size of the defect sought. "Size" here is some appropriate measure of the scale length of a defect that depends on its profile and circularity. For ease of visualization in the following discussion, assume that the defect is a circular lump that dies away within a radius r_L, giving the lump a size in mode number $m_L = \pi R/r_L$, where R is the sphere radius. Then assume this lump will be detected if a trace passes within $^2/_3\ r_L$ of the center of the lump. For the standard 9 trace measurement on an R=1 mm sphere, the probability of detecting such a lump (or equivalently, the percent coverage of the trace pattern) is ~33% for m_L = 10, only

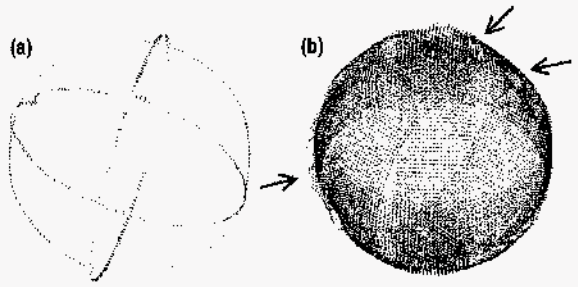

Fig. 2. Representation of the data taken by (a) the standard trace pattern—three paths with 10 μm separation along each of three mutually orthogonal great circles. (b) a complete coverage pattern—21 paths with 30 μm separation along four polar paths separated by 45° and one equatorial path. Some of the local depressions and maxima (magnified ~ 1000 times) revealed by these traces are indicated by arrows.

~10% for $m_L = 50$, and less, decreasing $\propto 1/m_L$, for higher modes (Fig. 3).

There were very practical reasons for such limited examinations. The first is time: every profile takes 1 min plus the 5–10 min needed for every shell re-orientation. Second is effort: the spheremapper used to take profiles has a radial dynamic range limited to ~5 μm [~10 μm in 2x range]; it can't move far off the high point on a sphere (the equator) without requiring careful manual readjustments.

We have made hardware and software changes to our spheremapper to take care of the second problem. We can now make measurements up to 330 μm from the equator

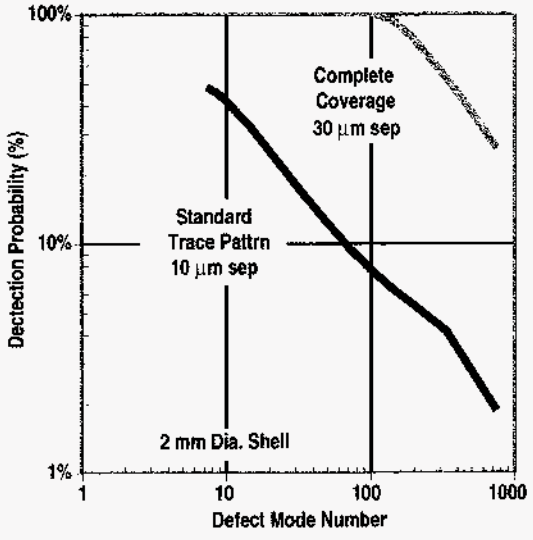

Fig. 3. Detection probability for a defect with size = m_L on a 2 mm dia shell using a standard trace pattern or a complete coverage pattern as shown in Fig. 2.

of a 2 mm diam shell without operator intervention. This is sufficient, with four manual reorientations, to give 100% coverage up to arbitrarily high m_L (*e.g.* no point on the shell is further from a trace than half the trace separation) [Fig. 2(b)]. The paths overlap at the poles (4 times) and equator (2 times), but no area is skipped. The time to take the 105 traces required for complete coverage using a 33 μm trace separation is only 2 1/2 h.

II. SPHEREMAPPER MODIFICATIONS

The Spheremapper contains two nearly independent computer systems; The AFM computer operates the atomic force microscope used for profiling and a motorized radial-displacement stage that automatically engages and disengages its tip. The Spheremap computer collects and analyzes the profile data, and operates the rotating vacuum chuck motor and a motorized z-displacement stage to center the AFM tip on the shell's equator and then offset the tip for parallel traces (Fig. 4). With this setup, the useful z-offset range is limited because the surface falls away as $1 - (1 - z^2/r^2)^{0.5}$; for a 2 mm diameter shell, a z-offset of 30 μm causes a shift equal to half the AFM range (~2 μm).

We have added a relay box to allow the Spheremap computer to temporarily take over the radial-displacement stage normally operated by the AFM computer, and modified the software so that the AFM tip can be moved along the curve of the shell. With this setup, the z-displacement is ~ 300 μm for a 2 mm diam shell, limited by interference between the base of the AFM tip and the shell (Fig. 5).

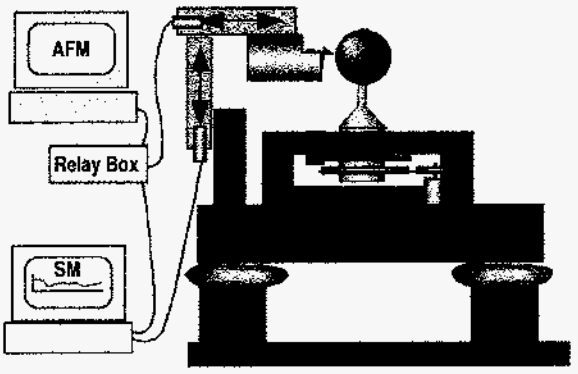

Fig. 4. Schematic of GA spheremapper setup. The AFM computer operates the AFM head and the radial-displacement stage used to engage and disengage the tip. The spheremapper computer collects angle and height information, and operates a z-displacement stage needed to make parallel traces. The relay box allows control of the radial-displacement stage by the spheremapper computer.

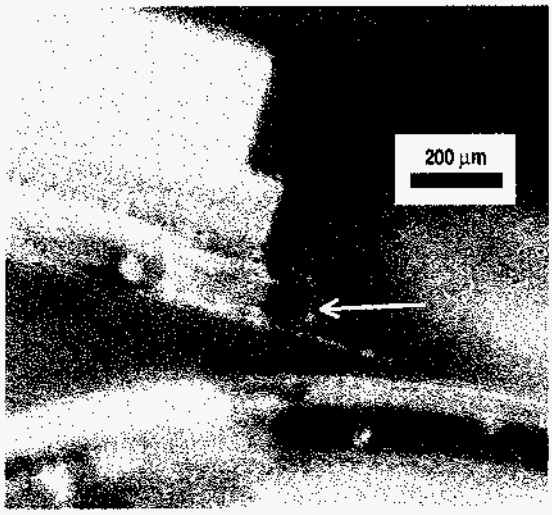

Fig. 5. Top image of AFM tip almost contacting a 2 mm diameter shell. The tip is at the end of a 200 μm long cantilever attached to a much larger glass block (its edge is shown with an arrow) about 50 μm from the surface of the shell.

III. MEASUREMENT ENHANCEMENTS

For our current procedures, the complete coverage trace pattern provides the basic information necessary for a good measure of the average fluctuation power spectrum (the average will be non-uniformly weighted over the shell surface as noted above) and the effort required to collect it is acceptable, at least for important shells. This information allows new possibilities also, if the points can be accurately registered relative to one another in the spherical coordinates θ and ϕ. That requires extreme care in re-orienting the shell on its vacuum chuck; there is always a slight bobble in picking up and replacing the shell that we estimate as typically <5°. This must be improved for accurate mapping.

It also requires registering the centers and radii of each measured circle relative to each other. The AFM head only measures fluctuations from circularity, not the radius of the circle. Our first estimate, the one used to calculate the image shown in Fig. 2(b), is to assume the data from each profile, $h(\phi, \theta=z/R)$ is centered around the same axis at the center of the shell, and that the radius of the profile = $R\cos(\theta)$. Neither assumption is necessarily true; a localized prominence in one profile shifts the apparent center relative to adjacent ones as does an asymmetric distortion (a tilted egg shape, for instance). The many intersections between curves provide enough information to self-consistently resolve this problem and we are working on an algorithm to implement it.

Even with modestly accurate mapping one could evaluate a shell's acceptability much more accurately by switching from Fourier to 1-D Wavelet transforms to describe the profiles.[4] The coefficients of the Fourier transform describes the amplitude of completely delocalized sin and cos functions, so give no spatial information about the local surface fluctuation power. Wavelet transforms convolute a profile with a localized perturbations of various wavelength. The amplitudes in those cases are spatially dependent, large only when coincident with a fluctuation of similar wavelength. One could sum the coefficients of wavelets of wavelength most important to RT instabilities, and use them to make a surface map of the sensitivity of the shell to instability during the implosion.

Accurate θ, ϕ registration of the profiles (uncertainty in radius and center less than the fluctuation amplitude), allows one to combine all the profile data to create an accurate $r(\theta,\phi)$ map of the surface. In this case, the 1-D wavelet transforms described above could be replaced with 2-D spherical wavelets,[5] perhaps allowing a better estimate of shell instability. It could, in addition, provide a sufficiently detailed description of the initial shell to model the implosion and make a detailed comparison of the simulated and experimental burns. This last possibility will need further development since it requires that a coordinate system be linked to each shell.

IV. SUMMARY

The GA Spheremapper mapping capability has been extended to allow 100% coverage with reasonable effort. This allows an accurate calculation of the average fluctuation power spectrum. It also allows evaluation of shells based on the distribution of fluctuation power in spherical coordinates, and could be used in the future as input to exactly simulate experimental implosions for stringent tests of ICF physics.

ACKNOWLEDGMENT

Work supported by U.S. Department of Energy under Contract DE-AC03-01SF22260.

REFERENCES

1. J.D. LINDL, *Inertial Confinement Fusion*, Springer-Verlag, New York (1998).
2. R.C. COOK, R. MCEACHERN, and R.B. STEPHENS, "Representative Surface Profile Power Spectra from Capsules Used in Nova and Omega Implosion Experiments," *Fusion Technol.* **35** 224 (1999).
3. S.W. HAAN, et al., Update on NIF Indirect Drive Ignition Target Specifications," *Fusion Technol.* **41** 224 (2002).

4. G.STRANG, "Wavelet transforms versus Fourier transforms," *Am. Math. Soc.* **28** 288 (1993).
5. P. SCHRöDER, W. SWELDENS, "Spherical Wavelets: Efficiently representing functions on a sphere," *Proc. of Siggraph 1995* pp. 161-195 (1995); software for making spherical wavelet transformations can be found at www.caltech.edu/software/sd/